MULTISCALE PROPERTIES OF TRAFFIC FLOW: THE MACROSCOPIC IMPACT OF TRAFFIC WAVES

NOUR KHOUDARI AND BENJAMIN SEIBOLD

Abstract. Vehicular traffic flow is a fascinating real-world system in which interactions at the vehicle scale, occurring on the scale of seconds, shape urban-scale flow patterns that develop over the scale of hours. A fundamental goal of traffic modeling is the development of mathematical equations that reproduce the fundamental laws that govern the flow behavior, without requiring detailed information about the human drivers or their vehicles. Starting from such models, it is shown how an additional scale can arise that lies between the microscopic vehicle scale and the macroscopic urban scale, namely: the mesoscopic scale of traffic waves. In certain flow regimes, uniform traffic flow is dynamically unstable, and small perturbations grow into traveling waves. Suitable models can quantify how this "phantom traffic jam" phenomenon lead to significant energy waste and reduction in flow efficiency. Moreover, via models and simulations, it is demonstrated how the introduction of a small number of automated vehicles can serve to recover the efficient uniform flow state.

1. Introduction

The modeling of vehicular traffic flow via principled mathematical equations is both a fascinating and challenging scientific endeavour, and an important building block for modern traffic simulation, forecasting, and control infrastructures. Many real-world systems that scientists aim to describe mathematically are either fully designed (by humans) or have undergone evolution (life science systems). Traffic flow falls in neither of these categories: while the roads and vehicles are designed, and drivers are instructed on the rules of the road, the emergent flow dynamics result from the collective behavior of the humans on the road—and they do so in intriguing ways, as we showcase here.

Any system that involves human agents is intrinsically challenging to model via principled equations, and care must be taken which aspects of the system one aims to reproduce and predict (see Perspective 2). For traffic flow on highways, it would be futile to want to forecast the precise trajectories of all vehicles, even if all vehicle positions were known at present. In contrast, it is very reasonable to predict the growth of a traffic jam, based on the knowledge of average vehicle flow rates along the highway, because that question is governed by a balance of flows rather than individual driving behavior.

The scale at which the individual vehicles move and interact is called the *microscopic* scale (lengths of up to 100m, and dynamics on the scale of seconds). In turn, the scale at which urban-scale traffic patterns (such as traffic jams and congestion patterns) form and dissipate is called the *macroscopic* scale (length of tens of kilometers, and time scales of tens of minutes to hours). Equilibrium traffic flow theory (§3) describes these large-scale patterns. In between these two scales, fascinating emergent structures can arise on a *mesoscopic* scale. In certain density regimes, dynamic instabilities can occur that push initially uniform flow into a regime dominated by traffic waves. This so-called "phantom traffic jam" phenomenon, i.e., unsteady traffic without any apparent cause, can arise due to the collective behavior of

the drivers [29, 21]. The instability and the development of waves have been demonstrated experimentally [56, 55]. These traffic waves tend to be 250–1000 meters long, and vehicles travel through the waves on a time scale of a minute. In traditional traffic measurements this mesoscopic waves scale is frequently missed (see Perspective 4). However, the large-scale effects of traffic waves can be significant in terms of wasted energy, accident risk, and also on flow efficiency. In this chapter we describe how these mesoscale structures can be reproduced via mathematical traffic flow, and how the connection across scales that the models provide yields an understanding of these waves.

Consistent with the different scales of traffic, different classes of models exist. Most prominently, *microscopic models* [50, 42, 4] directly describe the individual vehicles and their interactions via dynamical systems; in turn, *macroscopic models* describe the spatio-temporal evolution of the vehicle density (and other field quantities) via partial differential equations. The macroscopic models presented here are inviscid models [40, 52, 47, 48, 3]. However, various other types of macroscopic models also exist, whose structure enables different purposes. Examples are gas-kinetic [24, 49, 27], dispersive [35, 33], and viscous [30, 31] models.

In transportation engineering, microscopic models are commonly used for off-line simulations of specific scenarios (e.g., evacuations, impact of construction sites). The driver models can be calibrated to reproduce realistic traffic data [20, 4, 26, 21, 32, 23, 5], and are conceptually easy to adapt to complex scenarios such as a highly heterogeneous vehicle fleet. The fact that they produce trajectories for all simulated vehicles enables conclusions about individual vehicle and driver behavior.

In contrast, macroscopic models, or suitable cell-transmission model (CTM) discretizations thereof [8, 15, 9, 53], provide a natural framework for modeling large-scale traffic that in reality consists of millions of vehicles, via much fewer computational cells. Such models are well-suited for real-time state estimation [60, 64, 25] and control [45]. Because they describe traffic flow without resolving vehicles, they are compatible with many types of measurement data that avoid tracking individual vehicles (data privacy).

There are also mathematical connections between different types of models. For instance, microscopic [2], cellular [1], and gas-kinetic [27, 1] models converge to macroscopic models in certain suitable limits. However, due to the principal structural difference between microscopic and macroscopic models, they largely tend to be studied and applied in rather separate contexts. One important focus of this work is to partially bridge that divide and highlight some fundamental macroscopic consequences of traffic models that resolve scales below the macro scale: the vehicle scale and the waves scale.

This chapter is organized as follows. In §2, two fundamental types of traffic models, and some of their fundamental connections, are described: macroscopic and microscopic models. The theory of traffic flow in equilibrium conditions, i.e., the impact of large-scale flow balance, is described in §3, followed by non-equilibrium theory that includes dynamics governed by instabilities and waves, in §4. Then, in §5, via modeling, analysis, and simulations, it is demonstrated how the vehicle scale and waves scale manifest compared to the macro scale. Moreover, via models and simulations, it is demonstrated how a small number of automated vehicles can conduct flow smoothing control to recover the efficient uniform flow state. The chapter closes in §6 with a discussion.

Perspective 1. **Traffic flow terminology.**
Traffic flow theory relates fundamental quantities that describe the movement of vehicles. Considering (for simplicity) uniform vehicles of length ℓ, that travel with velocity v, we outline the following quantities.

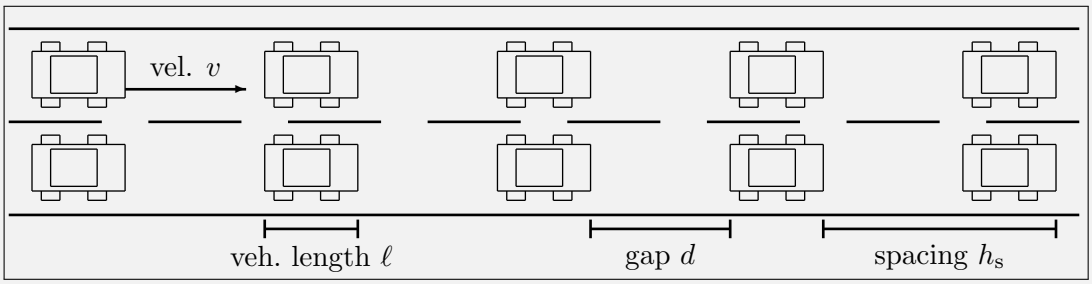

- The *spacing* h_{s} is the road length per vehicle.
- The *gap* $d = h_{\mathrm{s}} - \ell$ is the distance between vehicles.
- The vehicle *density* ρ is the number of vehicles per unit length.
- The *time headway* h_t is the time between two vehicles passing a fixed position.
- The *flow rate*, or *throughput*, q is the number of vehicles passing a fixed position per time.
- Spacing and density relate via $\rho = 1/h_{\mathrm{s}}$, and likewise flow rate and time headway relate via $q = 1/h_t$, and moreover $q = \rho v$.

2. Traffic Models

Here we present the fundamental principles of macroscopic (§2.1) and of microscopic (§2.4) traffic models, and outline some important examples of macroscopic (§2.2) and microscopic (§2.5) models. We also highlight properties of macroscopic models (§2.3), and show how to reconstruct macroscopic quantities from microscopic models (§2.6).

2.1. **Fundamental conservation principle.** Consider a segment of highway $x \in [a, b]$, devoid of any ramps. Consistent with the definition of vehicle density ρ, the number of vehicles (allowed to be non-integer in these fluid-dynamical models) in the segment $[a, b]$ is $m(t) = \int_a^b \rho(x, t)\,\mathrm{d}x$. That number $m(t)$ changes in time precisely by (i) vehicles entering the segment (at $x = a$) at a flow rate $q(a, t)$ and (ii) vehicles exiting the segment (at $x = b$) at a flow rate $q(b, t)$. Hence, it holds:

$$\int_a^b \frac{\partial \rho}{\partial t}(x, t)\,\mathrm{d}x = \frac{\mathrm{d}}{\mathrm{d}t} m(t) = q(a, t) - q(b, t) = -\int_a^b \frac{\partial q}{\partial x}(x, t)\,\mathrm{d}x\,. \tag{1}$$

Here the middle equality encodes flow conservation, while the first and third equality are basic facts of calculus. Because (1) holds for any choices of a and b, one obtains the *continuity equation*

$$\rho_t + q_x = 0\,, \tag{2}$$

which is a fundamental principle common to many flows (not just traffic). In (2), and below, subscripts denote partial derivatives, e.g., $\rho_t = \frac{\partial \rho}{\partial t}$. Moreover, the arguments (x, t) are frequently omitted for notational efficiency.

The ratio of flow rate and density is the *bulk velocity* of the flow

$$u = \frac{q}{\rho} \, .$$

In single-lane traffic, this u is identical to the vehicle velocity; however, a bulk velocity can also be defined for multi-lane traffic (alike an effective flow velocity of water in a river that can be defined even though the water flows faster near the center than near the shores). With that, the continuity equation (2) can also be written as

$$\rho_t + (\rho u)_x = 0 \, . \tag{3}$$

This equation is a key building block for all macroscopic traffic models.

2.2. **Formulating closed macroscopic traffic models.** Equation (3) by itself is not a model, (a) because it merely encodes a conservation principle, and (b) because it is a single equation for two fields, $\rho(x,t)$ and $u(x,t)$. In order to make (3) into a traffic model, another relationship has to be provided.

One way to do so is to postulate a functional relationship between vehicle density and bulk velocity, $u = U(\rho)$, or equivalently, between density and flow rate, $q = Q(\rho) = \rho U(\rho)$. The latter relationship is directly related to the fundamental diagram (see §3). This turns (3) into the *Lighthill-Whitham-Richards (LWR) model* [40, 52]

$$\rho_t + Q(\rho)_x = 0 \, , \tag{4}$$

which is a scalar hyperbolic conservation law.

Another possibility to close the model is to provide a second equation for the field variables, most naturally an evolution equation for the bulk velocity field. One such model is the *Aw-Rascle-Zhang (ARZ) model* [3, 66], which is a special case of generic macroscopic second-order models [36, 11]. In non-conservative velocity form the ARZ model reads as

$$\begin{aligned} \rho_t + (\rho u)_x &= 0 \, , \\ u_t + u u_x &= \rho h'(\rho) u_x + \tfrac{1}{\tau}(U(\rho) - u) \, . \end{aligned} \tag{5}$$

Here $h(\rho)$ is the *hesitation function*, and $U(\rho)$ is the *desired velocity function*. As in [51], $U(\rho)$ is strictly decreasing, the flow rate function $Q(\rho) = \rho U(\rho)$ is strictly concave, $h(\rho)$ strictly increasing, and $\rho h(\rho)$ strictly convex. In (5), the continuity equation (3) is augmented by a model for the vehicle acceleration $u_t + u u_x$, which is the sum of two terms: (a) the spatial gradient of the velocity field, weighted by $\rho h'(\rho)$, modeling the tendency to accelerate (decelerate) when traffic ahead is going faster (slower); and (b) the difference between the desired velocity $U(\rho)$ and the current velocity u. While the model (5) can also be formulated without this last relaxation term (i.e., $\tau \to \infty$) [3], and that formulation already renders the model more accurate on reproducing real data than the LWR model [12], it is the presence of the relaxation term [18] that allows for dynamic instabilities. While the form (5) is intuitive, it is the conservative form

$$\begin{aligned} \rho_t + \left(y - \rho h(\rho)\right)_x &= 0 \, , \\ y_t + \left(\tfrac{y^2}{\rho} - y h(\rho)\right)_x &= \tfrac{1}{\tau}(\rho(U(\rho) + h(\rho)) - y) \, , \end{aligned} \tag{6}$$

that is to be used for analysis and numerical approximation. Here $y = \rho w$, where $w = u + h(\rho)$ can be interpreted as a vehicle/driver property that is moving with the flow.

2.3. **Properties of macroscopic traffic models.** The LWR (5) and ARZ (6) models are nonlinear hyperbolic conservation/balance laws. A key feature is that their weak solutions allow for traveling discontinuities whose dynamics are described by jump conditions that follow from the conservation principles [10]. These discontinuities can be interpreted as mathematical idealizations of rapid transition zones (e.g., strong braking) in the real system that are much thinner than the problem's length scale of interest.

The LWR model (4) can be understood and solved (in certain setups, otherwise the numerical methods outlined in Perspective 3 can be used) via two fundamental principles:

(A) The *method of characteristics*. In a moving frame of reference $x(t)$ that moves with a speed $\dot{x}$, assuming a smooth solution of (5), the rate of change of density is

$$\frac{\mathrm{d}}{\mathrm{d}t}\rho(x(t),t) = \rho_t + \rho_x \dot{x}(t) = (\dot{x} - Q'(\rho))\rho_x \, .$$

Hence, if one chooses $\dot{x} = Q'(\rho)$, one has that $\rho(x(t),t) = \text{const.}$. This means that along lines $x(t) = x_0 + Q'(\rho(x_0,0))t$, the solution is constant. In other words, an initial profile $\rho(x,0)$ evolves under (5) as follows: each point (x,ρ) of the initial solution curve moves in x by its *characteristic velocity* $\dot{x} = Q'(\rho)$, while retaining its value ρ. This construction of the solution forward in time works until the solution curve ceases to be a smooth function. This breakdown of a classical solution generally occurs in finite time when $Q(\rho)$ is nonlinear and the initial profile is decreasing somewhere [10].

(B) The *Rankine-Hugoniot shock conditions* and *entropy conditions*. Beyond the breakdown of smooth (classical) solutions, weak solutions of (5) can be defined that allow for traveling discontinuities [10]. In order to preserve the conservation of vehicles, a discontinuity connecting two states ρ_L and ρ_R must move at the speed

$$s = \frac{Q(\rho_\mathrm{R}) - Q(\rho_\mathrm{L})}{\rho_\mathrm{R} - \rho_\mathrm{L}} \, . \tag{7}$$

A graphical interpretation of (7) is that the speed of that traveling discontinuity equals the slope of the secant line to the fundamental diagram curve $(\rho, Q(\rho))$ that connects the two points $(\rho_\mathrm{L}, Q(\rho_\mathrm{L}))$ and $(\rho_\mathrm{R}, Q(\rho_\mathrm{R}))$ (see the solid line shown in Fig. 2). In addition, traveling discontinuities are only admitted as feasible weak solutions if they are stable with respect to infinitesimal amounts of smearing (then they are called *shocks*). For the LWR model, this so-called *entropy condition* is equivalent to the requirement that the characteristic velocity at the left of the shock is larger than the characteristic velocity at the right, i.e., $Q'(\rho_\mathrm{L}) > s > Q'(\rho_\mathrm{R})$.

These two principles hold for a wide class of flux functions $Q(\rho)$. For the traffic flow models here, the function $Q(\rho)$ is assumed concave ($Q''(\rho) < 0$). Moreover, $Q(0) = 0$ (no vehicles means no flow), and $Q(\rho_\mathrm{max}) = 0$, modeling vehicle stoppage for some jamming density ρ_max (usually bumper to bumper plus some safety buffer). Under these assumptions there is a critical density ρ_c at which the flow is maximal (that flow $q_\mathrm{c} = Q(\rho_\mathrm{c})$ is called the *capacity* of the road). Moreover, for densities $0 \leq \rho < \rho_\mathrm{c}$, called the *free flow regime*, the characteristic velocity $Q'(\rho) > 0$. In turn, for densities $\rho_\mathrm{c} < \rho \leq \rho_\mathrm{max}$, called the *congested regime*, the characteristic velocity $Q'(\rho) < 0$, i.e., information travels backwards along the road.

For the ARZ model (6), analogous jump and Lax-entropy conditions can be formulated, in line with the standard theory of systems of hyperbolic conservation laws. We do not explicitly discuss them here, but they can be found in [3].

Perspective 2. **"All models are wrong, but some are useful."**
This aphorism, popularized by statistician George E. P. Box, is highly relevant for modeling traffic flow. For instance, assume the objective is to provide a principled predictor for the traffic densities and flow rates along a highway for the upcoming 15 minutes, given knowledge of the current density states. Then the fluid-dynamical LWR model (4) can be very useful, even though it captures neither variations in driver behavior, nor multi-lane effects. In contrast, if the objective is to predict the precise positions of all vehicles in 15 minutes, given the current positions of all vehicles, then any fluid-dynamical model will not be useful. For that objective, a detailed microscopic model with lane changing dynamics may achieve the goal. However, such a more detailed model would require information/data about the drivers' behavior—which are frequently not available in practice.
Hence, it is crucial to have a whole portfolio of traffic models available, and choose the right model detail appropriate for the questions and data at hand. Furthermore, we must keep in mind that some questions are fundamentally beyond reach (see also Perspective 5). For example, asking for a model that predicts the precise position of all vehicles after an hour of highly volatile city traffic is as futile as it is to predict the precise position of each grain of sand after an hour of a sand storm. In contrast, asking for a prediction of expected average commute times is as reasonable as it is to ask for the expected amount of sand being moved by the storm.

2.4. **Microscopic car-following models.** Consider vehicles at positions $\cdots < x_{j-1} < x_j < x_{j+1} < \dots$ along a single lane of highway, i.e., vehicle j follows vehicle $j+1$. Its gap ahead is $d_j = x_{j+1} - x_j - \ell$, and the velocity difference from the lead vehicle is $\dot{d}_j = \dot{x}_{j+1} - \dot{x}_j$. Here we describe simple car-following models that, in their basic form, are devoid of delays and noise.

A first-order traffic model is one where the vehicle velocity is specified directly, such as $\dot{x}_j = V(d_j)$, where $V(d)$ is a velocity–gap relationship (that can be constructed similarly to the velocity functions $U(\rho)$ in the macroscopic models (4) or (5)). With a density reconstruction as in §2.6 one obtains the LWR model (4) from such a first-order microscopic model. These first-order models do not exhibit instabilities, and thus they do not possess a mesoscopic waves scale.

The desired mesoscopic behavior *can* be achieved via *second-order car-following models* of the form

$$\ddot{x}_j = f(d_j, \dot{d}_j, v_j) \,, \tag{8}$$

which describe the acceleration of a vehicle as a nonlinear function of its gap ahead, its velocity difference from its leader, and its own velocity. Applying this model (8) for each vehicle means that the microscopic car-following model becomes a system of ordinary differential equations (ODEs) that dictates the motion of all vehicles on the road. The function f must be chosen to reproduce reasonable and realistic behavior, particularly avoiding collision whenever possible and maintaining realistic space and time gaps. In §4.1 we derive under which circumstances instabilities in such models arise, and in §5 we showcase the resulting waves via simulations.

2.5. **Optimal velocity model.** An important example of a second-order car-following model is the *optimal velocity model* (OVM), introduced in [4]. It is a special case of (8) that bases the vehicle acceleration solely on the gap and ego velocity. Here we augment the OVM

with a follow-the-leader term to guarantee braking in reaction to velocity differences to avoid collisions. The resulting model used herein (and for simplicity just denoted OVM), reads as

$$f(d_j, \dot{d}_j, v_j)_{\mathrm{OVM}} = a\,[V(d_j) - v_j] + b\left[\frac{\dot{d}_j}{(d_j)^\nu}\right]. \tag{9}$$

Here $V(d)$ denotes the optimal velocity function, determined by the gap to the vehicle ahead, which is chosen to be a monotone increasing, continuous, non-negative function which is zero for some minimum gap d_0 and asymptotes at a maximum velocity v_0 for $d \to \infty$. Besides that function $V(d)$, the model has three further free parameters: the sensitivity $a > 0$, describing the importance of adherence to the optimal velocity; the braking coefficient $b > 0$, capturing the importance of equilibrating one's own velocity to the leader's velocity; and the exponent $\nu > 0$, affecting how long-ranged vs. short-ranged the impact of the velocity-equilibration will be. Because the follow-the-leader term is singular for $d \to 0$, the model avoids vehicle collisions; however, unrealistically large decelerations are not excluded from occurring.

For all the microscopic simulations and results in §5, we use the model (9), with $a = 1.3\frac{1}{\mathrm{s}}$, $b = 15\frac{\mathrm{m}^2}{\mathrm{s}}$, and $\nu = 2$. Moreover, the optimal velocity function is chosen to be

$$V(d) = c\,\frac{-d_0 + \sqrt{d_0^2 - (d_0^2 - d^2)(c^2\frac{d^2}{v_0^2} + 1)}}{c^2\frac{d^2}{v_0^2} + 1}\,, \tag{10}$$

where $d_0 = 2\mathrm{m}$ is the minimum gap, $v_0 = 30\frac{\mathrm{m}}{\mathrm{s}}$ is the maximum velocity, and $c = \frac{1}{\mathrm{s}}$.

The OVM used herein is one specific example of a class of car-following models. It is chosen due to its analogy to the ARZ model (5) that also models vehicle accelerations as a combination of velocity equilibration and optimal-velocity relaxation. A wide variety of other car-following model exists. For example, the *intelligent driver model (IDM)* [57, 22] is capable of producing the same types of features like dynamic instabilities around equilibrium states.

2.6. **Transitioning scales: macroscopic fields from microscopic trajectories.** Given N vehicles at positions $x_j(t)$ for $j = 1, \dots, N$, that travel at velocities $\dot{x}_j(t)$, macroscopic field quantities can be constructed via the kernel density estimate

$$\rho(x,t) = \sum_{j=1}^{N} G(x - x_j) \quad \text{and} \quad q(x,t) = \sum_{j=1}^{N} \dot{x}_j G(x - x_j)\,. \tag{11}$$

Here G is a kernel, such as a Gaussian $G(x) = (\sqrt{\pi}h)^{-\frac{1}{2}} \exp(-(x/h)^2)$. The "smoothing length" h needs to be chosen to be larger than the typical spacing between vehicles but smaller than the macroscopic length scales of interest. As straightforward differentiation reveals, formulas (11) guarantee that the reconstructed fields satisfy the continuity equation (2) exactly.

This kernel density estimation can be used to reconstruct effective average solutions at different macroscopic scales. In §5, we run a micro simulation and reconstruct two density solutions using (11) for two different values of h. The first reconstruction is averaging over the vehicle scale with $h = 25\mathrm{m}$ but it is fully resolving the traffic waves that arise; in turn, the second reconstruction is averaging over the waves scale with $h = 1000\mathrm{m}$, and is therefore yielding the effective densities and flow rates on the largest scales.

Perspective 3. **Intuitive ways to interpret and compute traffic models.**
The simplest way to computationally approximate microscopic models, like (8), that come in the form of ordinary differential equations, is via Euler's method, as follows. First, (8) is written in position–velocity form as

$$\begin{aligned} \dot{x}_j &= v_j \ , \\ \dot{v}_j &= f(x_{j+1} - x_j, v_{j+1} - v_j, v_j) \ . \end{aligned}$$

Second, a suitably small time step $\Delta t > 0$ is introduced, and the rates of change $\dot{x}_j$ and $\dot{v}_j$ are approximated by the discrete update rule

$$\begin{aligned} x_j^{n+1} &= x_j^n + \Delta t v_j^n \ , \\ v_j^{n+1} &= v_j^n + \Delta t f(x_{j+1}^n - x_j^n, v_{j+1}^n - v_j^n, v_j^n) \ , \end{aligned}$$

which takes the positions x_j^n and velocities v_j^n of all vehicles at time step n, and uses them to construct the positions and velocities at the new time step $n+1$.

Macroscopic models, like the LWR model (4), can be approximated numerically in a similar spirit. In addition to the time step Δt, the road must also be divided up into cells of size Δx. On the j-th cell, at time step n, the quantity ρ_j^n denotes the average density of vehicles on that cell.
Given all the cell densities ρ_j^n at a given time step n, we first calculate the fluxes of vehicles through all boundaries between adjacent cells. For instance, the flux from cell j into cell $j+1$ is obtained as follows. The maximum flow that cell j can send is given by $Q_{\mathrm{S}}(\rho_j^n)$, where the sending function $Q_{\mathrm{S}}(\rho) = Q(\min\{\rho, \rho_{\mathrm{c}}\})$ agrees with the flux function $Q(\rho)$ in free flow and is maximal in congestion. Here ρ_{c} is the critical density, as described in §2.3. The receiving function $Q_{\mathrm{R}}(\rho) = Q(\max\{\rho, \rho_{\mathrm{c}}\})$ is the reverse, and the maximum flow that cell $j+1$ can receive is $Q_{\mathrm{R}}(\rho_{j+1}^n)$. The actual flux is then $F_{j+\frac{1}{2}} = \min\{Q_{\mathrm{S}}(\rho_j^n), Q_{\mathrm{R}}(\rho_{j+1}^n)\}$, and the update rule for each cell is

$$\rho_j^{n+1} = \rho_j^n + \frac{\Delta t}{\Delta x}(F_{j-\frac{1}{2}} - F_{j+\frac{1}{2}}) \ .$$

This approximation, which is equivalent to *Godunov's method* [16], is the basis for cell-transmission models (CTMs) [8, 15]. Similar in spirit, albeit more intricate, methods can also approximate second order macroscopic models, like the ARZ model (6) via the 2CTM [13].

3. Equilibrium Traffic Theory and the Fundamental Diagram

3.1. **The fundamental diagram of traffic flow.** The central property of equilibrium traffic flow is the relationship between vehicle density and velocity, $u = U(\rho)$, or equivalently between density and flow rate $q = Q(\rho)$ (see §2.2). Based on the continuity equation (2), the LWR model (4) was derived.

The relationship between density ρ and flow rate q is called the *fundamental diagram (FD) of traffic flow*. Many forms of measurements or models of the FD have been conducted or proposed [19, 40, 17, 58, 43, 8, 60, 12, 11]. Most prominent are the first measurements by Greenshields [19], see Perspective 4. While Greenshields's data hinted at a rather well-defined functional relationship $q = Q(\rho)$, subsequent and contemporary measurements of the FD show

a more complicated picture: while for low densities a reasonable direct relationship is present, near and above the critical density ρ_c, the data exhibit a significant spread [29], also shown via the data in Fig. 1. While the LWR model cannot reproduce this FD spread, many types of more sophisticated models do capture [7, 12, 11] or even explain [54] the spread.

In the "OVM equilibrium curve" in Fig. 1, the two characteristic densities are $\rho_{\max} = 143.3\,\text{veh/lane/km}$ and $\rho_c = 39.5\,\text{veh/lane/km}$. Moreover, the capacity is $q_c = 2194\,\text{veh/lane/h}$, which corresponds to a time-headway of 1.6 seconds. That is a tighter following than the 2-second rule that is frequently recommended to drivers, which is in agreement with general observations about real-world human driving.

Perspective 4. **Traffic measurements and data.**
The first traffic measurements were conducted by Bruce Greenshields [19]. In the 1930s, only a few decades after the first Ford Model T, he used an early video camera to measure vehicle speeds and densities and obtained the first empirical measurements of the fundamental diagram of traffic flow. Since the 1960s, many highways have been equipped with dedicated sensing infrastructure, like induction loop detectors, that measure vehicle flow rates, and also other quantities like vehicle velocities. These data have enabled transportation agencies to plan policies, and in some cases also assist real-time connected corridor management. With the wide adoption of smartphone technology (late 2000s), a huge surge in traffic data collection by private companies occurred. These data strongly focus on vehicle travel times.
Interestingly, despite these decades of widespread collection of traffic data, there remains a fundamental lack of quality data that would enable transportation scientists and engineers develop more accurate traffic models. The reason is that data are needed that capture driving reactions to other vehicles, for many vehicles over long road segments and time intervals. However, loop detector data lack the required resolution, as they are only collected at fixed locations; and smartphone data, if publicly available at all, lack information about the vehicles ahead and around the sensed vehicle. Due to these data challenges, huge leaps in past traffic modeling have been based on specific camera-based [59] or drone-based [34] data sets that provide trajectories of all vehicles on certain segments of roads. However, large-scale, long-term, high-resolution traffic data remain a critical need in traffic modeling [46].

3.2. **Large scale traffic patterns.** A typical setup where the LWR model produces clear non-trivial patterns is that of the sudden occurrence of a physical bottleneck on the road and the subsequent formation of a traffic jam. Consider at the initial time a road segment with a uniform free flow state, shaped by a steady inflow close to the road's capacity (the square in Fig. 2). Then, a bottleneck forms at one location (e.g., caused by a speed reduction, as in the scenario described in §5) which limits the admissible throughput to below the inflow rate. In Fig. 2 this outflow state is shown via the diamond. Due to the reduced speed it is below the equilibrium curve. Moreover, because the inflow rate exceeds the outflow rate, a congested state (the triangle in Fig. 2) arises, whose flow rate equals that of the bottleneck state, and the density lies on the congested arc of the equilibrium curve.

In line with the theory discussed in §2.3, the inflow state connects with the congested state (the "traffic jam") via a shock, which travels backwards along the road, at a speed equal to the slope of the line in the FD that connects the square with the triangle (Rankine-Hugoniot

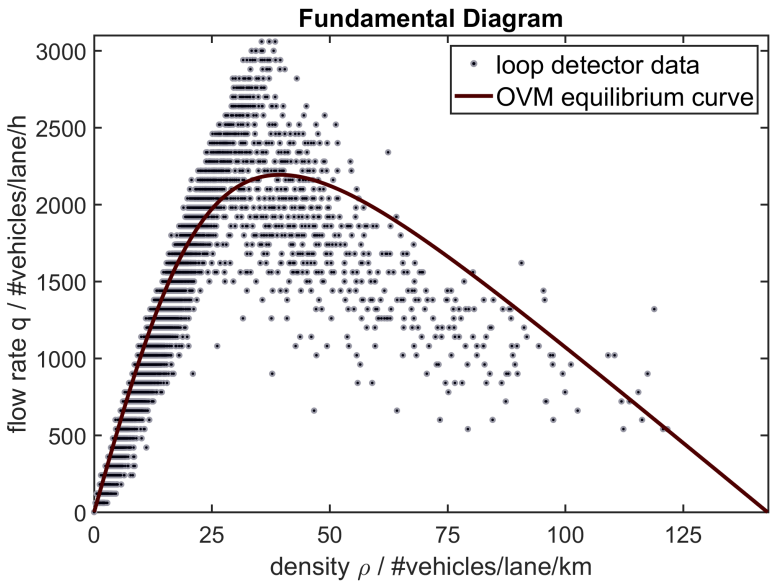

Figure 1. The fundamental diagram of traffic flow, displaying real detector data (as in [54]) together with the equilibrium density–flow rate relationship for the OVM used in this work. In congestion, the real data exhibit a characteristic spread, with many points being below the equilibrium curve.

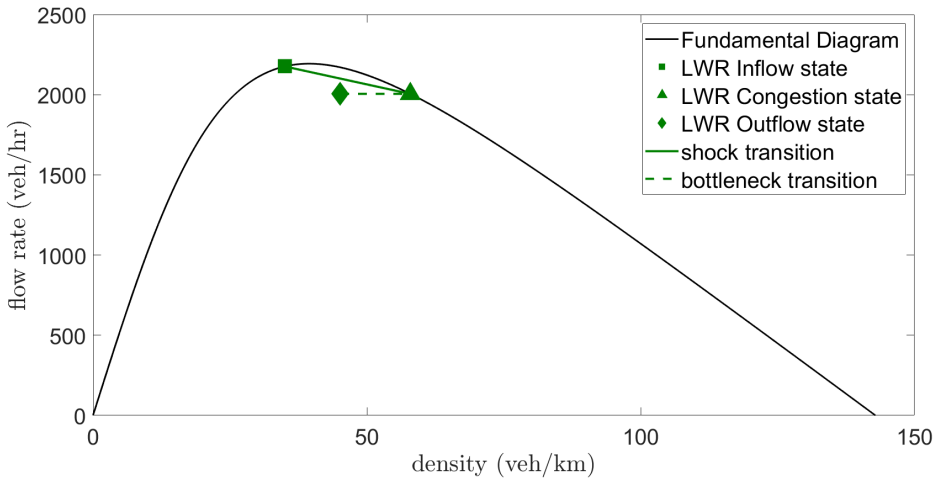

Figure 2. Fundamental diagram curve with LWR states, representing an inflow state (square) in free flow, a downstream outflow state (diamond) of reduced flow rate, and a congested state (triangle) induced by the bottleneck. The line connecting the inflow and congested state represents a shock with a slope equal to the shock's speed, due to (7). The line connecting the congested state with the outflow state represents the transition at the bottleneck.

condition (7)). Moreover, the line that connects the triangle with the diamond in Fig. 2 represents the transition at the bottleneck.

4. Non-Equilibrium Traffic Theory

4.1. **Dynamic instability of uniform flow.** For microscopic models, we consider the second-order car-following form (8), and assume that the function f is so that equilibrium solutions (i.e., those where all vehicles travel at steady speeds, $\ddot{x}_j = 0$) are precisely those where all vehicles are equi-spaced with identical velocities v^{eq}. It is important to note that not every car-following model satisfies this last assumption. For instance, the follow-the-leader dynamics $\ddot{x}_j = b\,\dot{d}_j/(d_j)^\nu$ (i.e., model (9) without the a-term) possess equilibria in which all vehicles travel at identical velocities, however not necessarily with equal spacing. In contrast, the models discussed in §2.5 do satisfy this assumption.

We now linearize the model (8) around a given equilibrium solution, by considering solutions $x_j = x_j^{\text{eq}} + y_j$, where $\frac{\mathrm{d}}{\mathrm{d}t} x_j^{\text{eq}} = v^{\text{eq}}$ and y_j is an infinitesimal perturbation. A Taylor expansion of f around the equilibrium state then yields the linearized dynamics

$$\ddot{y}_j = \alpha_1\,(y_{j+1} - y_j) - \alpha_2\,\dot{y}_j + \alpha_3\,\dot{y}_{j+1}\;, \tag{12}$$

where $\alpha_1 = \frac{\partial f}{\partial d}$, $\alpha_2 = \frac{\partial f}{\partial \dot{d}} - \frac{\partial f}{\partial v}$, and $\alpha_3 = \frac{\partial f}{\partial \dot{d}}$, all evaluated at equilibrium. Whether (12) induces stable or unstable behavior can now be analyzed via the *frequency response* of the car-following input-output behavior, as follows. Due to the linearity of (12) it suffices to study the behavior of basic waves. Specifically, we make the Laplace transform ansatz $y_j(t) = c_j e^{\omega t}$, where $c_j, \omega \in \mathbb{C}$. Substituting this into (12) allows us to write the j-th vehicles amplitude c_j in terms of its lead vehicle's amplitude c_{j+1} as

$$c_j = F(\omega) c_{j+1}\;, \quad \text{with the transfer function} \quad F(\omega) = \frac{\alpha_1 + \alpha_3\,\omega}{\alpha_1 + \alpha_2\,\omega + \omega^2}\;.$$

Here $\mathrm{Re}(\omega)$ describes the temporal growth/decay and $\mathrm{Im}(\omega)$ the frequency of oscillation of the perturbation signal. Moreover, $|F|$ describes the growth/decay of the perturbation amplitude from vehicle to vehicle, and the angle $\theta(F)$ captures the phase shift across vehicles.

The equilibrium solution of the car-following model (8) is now called *string stable* if $|F(\omega)| \leq 1$ for all $\omega \in i\mathbb{R}$, i.e., for stability it suffices to only consider perturbations that are purely oscillatory. As shown in [63], string stability happens exactly if

$$\alpha_2^2 - \alpha_3^2 - 2\alpha_1 \geq 0\;. \tag{13}$$

In turn, if (13) is violated, then some perturbations exhibit exponential growth, until nonlinearities via (8) transform them into traffic waves or other nonlinear non-equilibrium features.

For macroscopic models, the linear stability analysis of uniform flow can be carried out by calculating the growth rates of Fourier modes [30, 14]. For the ARZ model (5) consider a constant base state solution $\rho = \tilde{\rho}$ and $u = U(\tilde{\rho})$, and infinitesimal wave perturbations of the form

$$\hat{\rho} = \hat{R} e^{ikx+\sigma t} \quad \text{and} \quad \hat{u} = \hat{U} e^{ikx+\sigma t}\;,$$

where k is the wave number and σ the complex growth rate. Substituting the perturbed solution $\rho = \tilde{\rho} + \hat{\rho}$ and $u = U(\tilde{\rho}) + \hat{u}$ into (5), and considering only constant and linear terms yields the homogeneous linear system

$$\begin{bmatrix} \sigma + ikU(\tilde{\rho}) & ik\tilde{\rho} \\ \sigma U(\tilde{\rho}) + ikU(\tilde{\rho})h'(\tilde{\rho}) - \frac{1}{\tau}U'(\tilde{\rho}) & \sigma + ikU(\tilde{\rho}) + \frac{1}{\tau} \end{bmatrix} \begin{bmatrix} \hat{R} \\ \hat{U} \end{bmatrix} = \begin{bmatrix} 0 \\ 0 \end{bmatrix}, \tag{14}$$

for the perturbation amplitudes. Nontrivial solutions can only exist if the matrix in (14) has vanishing determinant, which determines the growth factor function $\sigma(k)$. That function can

then be shown to produce stable solutions, i.e., $\mathrm{Re}(\sigma) \leq 0$, exactly if

$$h'(\tilde{\rho}) + U'(\tilde{\rho}) \geq 0 \,. \tag{15}$$

This condition (15) can alternatively be obtained from the sub-characteristic condition [61, 62, 41, 6, 39], which states that the two characteristic speeds of the ARZ model (5) bracket the characteristic speed of the reduced LWR model (4) at the same equilibrium state $\tilde{\rho}$. Furthermore, a uniform base state of (5) is unstable exactly if nonlinear traveling wave solutions, so-called *jamitons*, exist [54].

Perspective 5. **Instability as a creator of structure.**
Much of the exciting structure that governs the natural (i.e., not human-made) world around us is shaped by instability. An equilibrium state, such as a uniform/flat situation, is called stable if small perturbations do not amplify. In turn, instability means that (certain) small perturbations do amplify and grow into non-small features. Commonplace mechanisms for instability are positive feedback loops, i.e., a small push of a system in one direction causes a subsequent tendency of the system to go further into that same direction.
An archetype example is a pendulum. Its two equilibrium states, i.e., hanging straight down and pointing straight upwards, fundamentally differ in terms of stability: a downward pendulum remains nearby under small perturbations; but an initially upwards pendulum will react to a small perturbation by departing from its upward state.
More exciting real-world examples of instabilities are the following. (A) **Surface waves on the sea** are caused by a shear instability: once a small crest forms, wind is more effective at pushing onto it, thus growing the crest. (B) **Sand dunes** grow because a small uphill slope makes wind-blown sand grains bounce uphill, thus growing the hump ("saltation"). (C) **Sea ice patterns** are strongly affected by the albedo difference: once melted, ice/water absorbs more sun radiation, thus amplifying the melting process. (D) **Defrosting food in a microwave oven**, if carried out too quickly, can produce boiling water next to ice, because microwaves heat water better than ice. (E) **Fluid dynamics** is a rich source of instabilities, such as a stream of water breaking up into droplets due to surface tension ("Plateau-Rayleigh instability"), or plumes forming when a denser fluid is placed above a lighter fluid ("Rayleigh-Taylor instability").

4.2. **Traveling wave solutions.** Consider a solution of the continuity equation (2) that is a single profile moving with speed s along the road ($s > 0$ means the wave moves forward, $s < 0$ means it moves backwards), i.e., the quantities ρ and q depend on a single variable $\eta = x - st$ only. Then $\rho_t = -s\frac{\mathrm{d}\rho}{\mathrm{d}\eta}$ and $q_x = \frac{\mathrm{d}q}{\mathrm{d}\eta}$, and thus (2) becomes $\frac{\mathrm{d}}{\mathrm{d}\eta}(-s\rho + q) = 0$. Integration yields $-s\rho + q = m$, where the integration constant m is the mass flux of vehicles relative to the wave. Thus one obtains the relationship

$$q = m + s\rho \,,$$

meaning that pairs of density and flow rate, (ρ, q), that satisfy (2) and are traveling waves, form straight lines in the fundamental diagram plane, where the line's slope s equals the speed of the traveling wave.

In the microscopic simulation results in §5, we employ density reconstructions, as in §2.6, to visualize data that exhibit such traveling wave behavior (see the red dots forming a straight line in Fig. 3). In macroscopic models, the nonlinear jamiton waves, and their formation

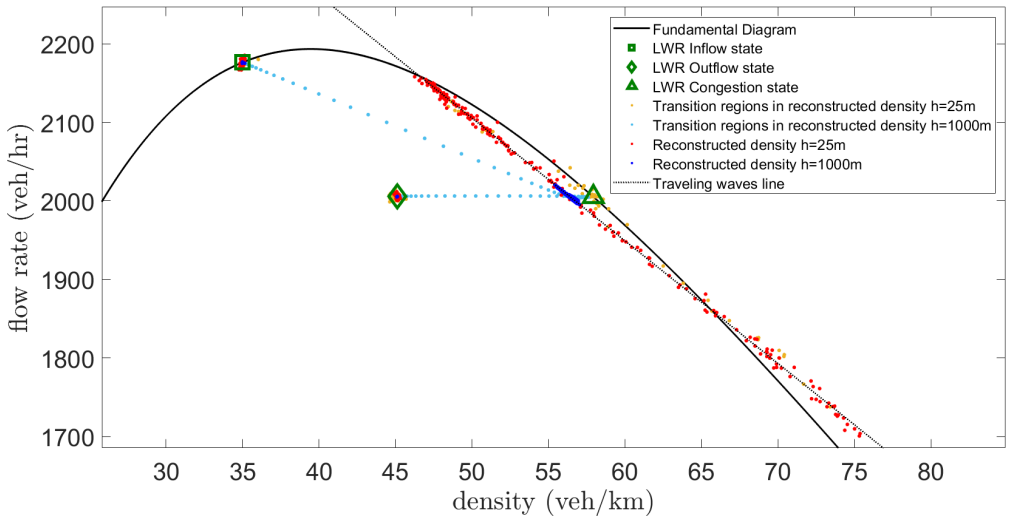

Figure 3. The density and flow rate of traffic states from a simulation, reconstructed on scales $h = 25$m (red, orange) and $h = 1000$m (blue, light blue), shown in the fundamental diagram graph, together with LWR inflow, congested, and outflow states (green symbols). The red dots show how traveling waves form a straight line, and the blue dots show how the effective traffic state falls below the equilibrium curve.

exactly when uniform flow is unstable, has been established [38, 28, 44, 14, 54]. Moreover, the way that jamitons form lines in the fundamental diagram has also been related to the observed spread the fundamental diagram [54].

5. Traffic Scenarios Governed by all Relevant Scales

5.1. **A concrete traffic jam scenario.** We consider a 40km road with a bottleneck at milestone 35km resulting from a restriction on the maximum speed allowed. The sudden decrease in maximum speed from $v_0 = 30\frac{\text{m}}{\text{s}}$ to $v_0 = 22.5\frac{\text{m}}{\text{s}}$ induces a modified outflow condition downstream of the bottleneck (which is now on a different fundamental diagram), and a congested region (a traffic jam) starts to form and grow upstream of the bottleneck. As time advances, the jam continues to grow backwards further and further, with the usual undesirable consequences such as spillback effects onto ramps further upstream.

We run a micro simulation for this scenario for up to 200 minutes after the bottleneck occurrence. We use the model (9) for all vehicles, and use a ballistic integrator to numerically solve the ODEs, with time step $\Delta t = 0.25$s. Moreover, to trigger any instabilities that may be present, we augment (9) with a noise term that is scaled so that the impact of the noise over a time interval is a normally distributed random perturbation with mean zero and variance $\sigma^2 = (0.05\frac{\text{m}}{\text{s}})^2$ times the interval's length.

5.2. **Instabilities and traffic waves across scales.** The model and simulation parameters are chosen so that the congested state that is caused by the bottleneck is unstable and thus small perturbations (triggered by the noise) will amplify (see §4.1) and grow into traveling waves. At the microscopic vehicle interaction scale, these waves in the congested region can be seen via a reconstruction of density and flow rates (§2.6) using a smoothing length (here:

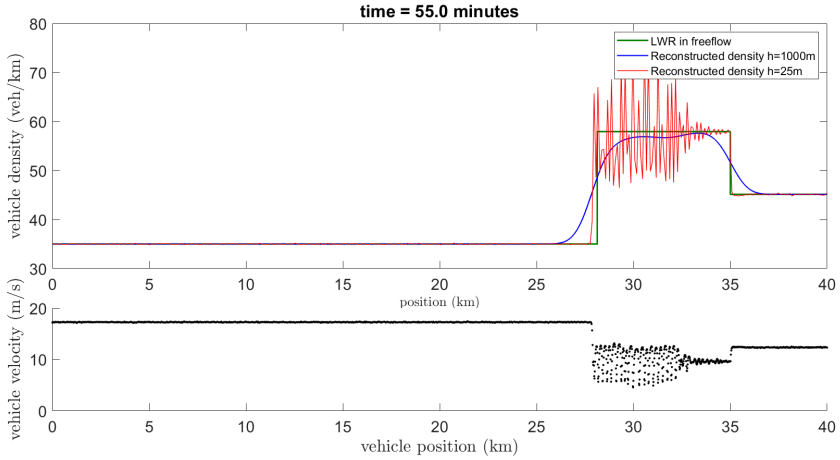

(a) Traffic state soon after bottleneck occurrence, when waves have started to develop.

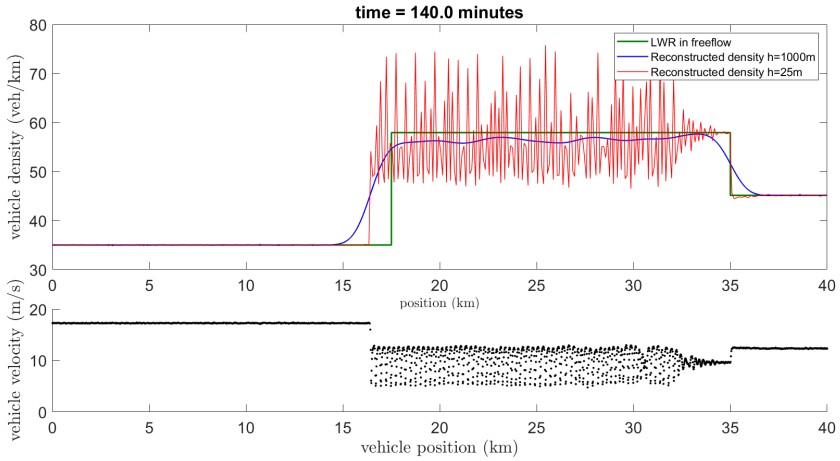

(b) Traffic state at some later time, with many full-grown waves.

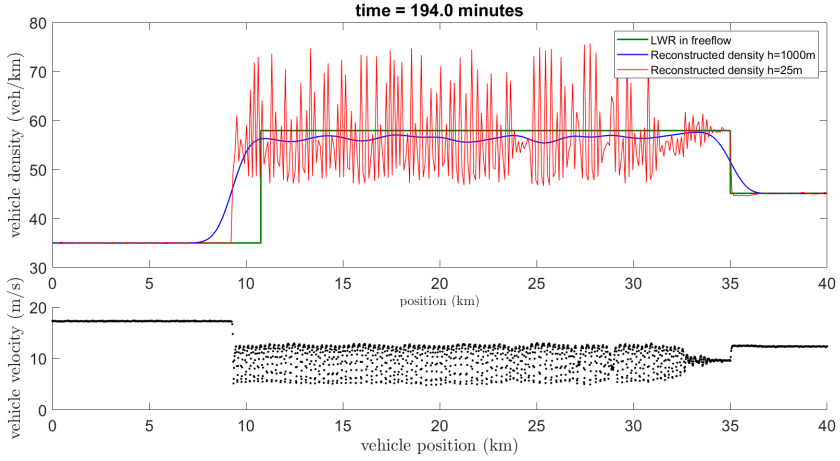

(c) Traffic state at a large final time, with a long jam dominated by waves.

Figure 4. Plot of the traffic states after three different times ((a), (b), (c)). At each time, the vehicle positions and velocities are shown (bottom), and (top): the vehicle density, reconstructed with two different smoothing lengths ($h = 25$m and 1000m), together with the LWR solution for the same setup.

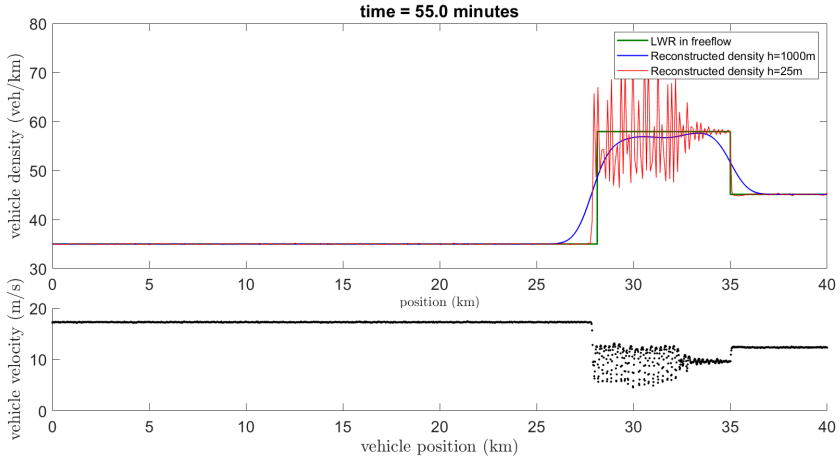

(a) Traffic state soon after bottleneck occurrence, with no AVs active yet.

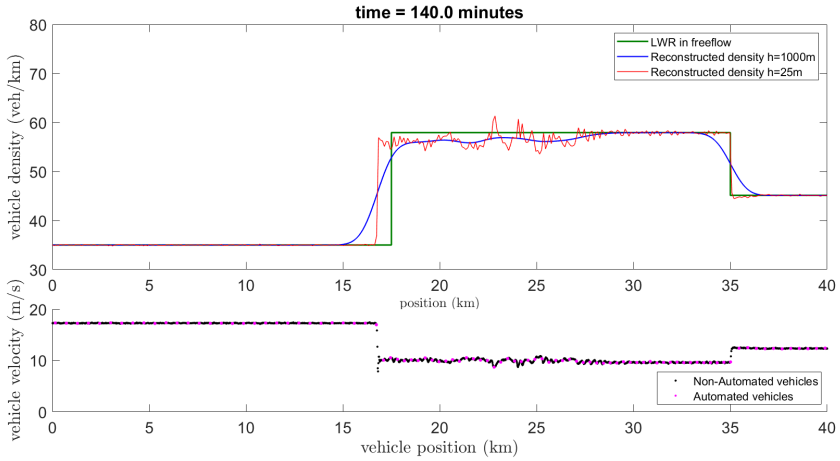

(b) Traffic state at some later time, after AV control has been activated.

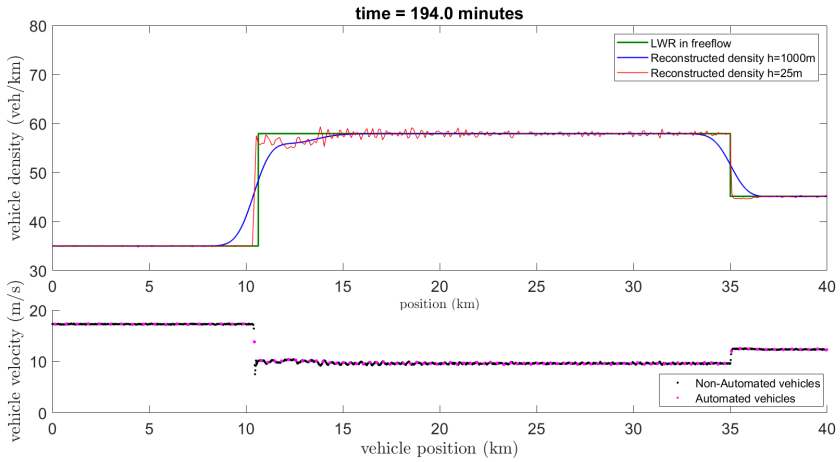

(c) Traffic state at a large final time, after AVs had time to fully dampen the waves.

Figure 5. Plot of the traffic states at the same times as in Fig. 4a, Fig. 4b, and Fig. 4c, plotted with the same reconstructions. However, now at $t = 97$ minutes, the wave smoothing controllers of the AVs (5% penetration rate) are activated.

$h = 25$m) that is small enough to average over vehicles but wide enough to still capture the mesoscopic waves scale.

In contrast, the choice of a smoothing length (here: $h = 1000$m) that is larger than the typical wave length but shorter than the road length, yields a macroscopic reconstruction that does not anymore capture the mesoscopic waves scale. The resulting reconstruction reveals the effective vehicle densities and flow rates that occur in the presence of waves.

Finally, one can also consider the LWR states that would arise if no instabilities were present. This construction, described in §3.2, would also be (approximately) recovered by reconstructions of microscopic models, if these models did not exhibit any instabilities. However, because instabilities do arise here, the wave-averaged reconstructions of the microscopic simulation can be expected to *not* match the LWR states.

The results of the simulation of the described scenario are shown in Figs. 4a–4c. In each figure, the density reconstructions on different scales ($h = 25$m via the red curve, and $h = 1000$m via the blue curve) are shown, together with the LWR reference state (green curve). Figure 4a shows a state soon after the bottleneck occurrence, when waves have just started to develop, Fig. 4b represents an intermediate phase where waves have developed, and Fig. 4c shows a large final time at which a long jams has formed.

The fine reconstruction (red curves) that resolves the mesoscopic waves scale shows that significant waves form in the congested region with densities and velocities oscillating around the LWR reference states. Moreover, the wave-averaged reconstruction (blue curves) shows that the effective average density in the presence of strong waves is in fact *not* identical to the LWR congestion state. Instead, the waves manifest in a reduced average density (the constant braking and accelerating causes each vehicle, on average, to take up more space than what uniform traffic would require); and that reduced non-equilibrium density state causes the traffic jam to become longer (by about 1.5km at the final instance in time) than what would happen under equilibrium conditions.

An additional feature that can be observed in the simulation results is that the waves do not reach their full strength instantaneously. Instead, they are shed just upstream of the bottleneck and grow as they travel backwards. As a consequence, there is a region, upstream of the bottleneck, at which the waves are small and the wave-averaged reconstruction (blue curve) almost matches the LWR state. However, as the jam grows this region becomes less and less relevant.

5.3. **Manifestations of instabilities and waves in the fundamental diagram.** For the micro simulation described above, in addition to the reconstructed densities discussed in §5.2, the corresponding flow rates can be reconstructed as well, as described in (11). This yields pairs in the (ρ, q)-domain that provide further insights about waves at the level of the fundamental diagram. Figure 3 shows the spread of those data points in the fundamental diagram domain, reconstructed from the simulation state shown in Fig. 4c. The red and blue dots in Fig. 3 are the (ρ, q)-pairs resulting from the two reconstructions, $h = 25$m and $h = 1000$m, respectively, inside the three LWR regimes. Moreover, the dots in orange and light blue correspond to the transition zones for both reconstructions, around the shock and the bottleneck. Specifically, the transition zones are defined as the regions where the density reconstruction with $h = 1000$m exhibits smeared transitions, combined with the regions where the waves from the reconstruction with $h = 25$m have not fully developed yet near the bottleneck or where they start to fade away near the shock. These transition region points

(orange and light blue) are displayed for completeness, but the red and blue points are the relevant data to understand the impact of waves.

The results in Fig. 3 show that the reconstruction that averages over the vehicle scale (red dots) and the reconstruction that averages over the wave scale (blue dots) both match the LWR solution for the inflow free flow region (clusters under the green square on the FD), as well as for the outflow region (clusters under the green diamond). In contrast, for the congested region, the red dots exhibit a significant spread, forming (almost precisely) a straight line (compare with the fitted dashed line). In line with the derivation in §4.2, this fact indicates that those waves are indeed traveling waves, moving backwards along the road at a speed equal to the slope of the line that is formed by the data points in the FD.

Meanwhile, the blue dots corresponding to the congested region form a cluster at a point underneath the equilibrium curve, which lies in between the LWR congestion state (green triangle) and the outflow state (green diamond). This shows that a wave-dominated congested traffic state has an effective (i.e., wave-averaged) throughput that equals that of the LWR congested state (and also the LWR outflow state), but it has a reduced density. As already mentioned in §5.2, this fact can be interpreted as unsteady traffic requiring more space than steady traffic, resulting in undesirable spill-back effects along the highway—a highly relevant macroscopic consequence of meso-scale waves features that are caused by micro-scale vehicle interactions.

5.4. **The impact of flow smoothing via vehicle automation.** The experiment in [55] has demonstrated that a few automated vehicles (AV) in the traffic stream can dampen waves and recover a stable and fuel-efficient uniform flow [65], even if the human drivers retain their intrinsically unstable driving behavior. Here we study in simulation how such sparse Lagrangian AV-based flow controls would affect the situation shown in Fig. 4b and Fig. 4c. An example of the analogous simulation is shown in Figs. 4a–4c, but now with 5% of the vehicles being made into AVs. The control law describing the AVs in this simulation is the OVM model (9), augmented with an additional relaxation term, reading as

$$f(d_j, \dot{d}_j, v_j)_{\mathrm{AV}} = f(d_j, \dot{d}_j, v_j)_{\mathrm{OVM}} + \gamma(U - v_j)\ . \tag{16}$$

Here γ is the control gain, and U is a fixed desired velocity towards which AVs are relaxing their own speeds. In this simulation, we set $\gamma = 1\frac{1}{\mathrm{s}}$ and $U = 9.6135\frac{\mathrm{m}}{\mathrm{s}}$, as determined by the LWR congested state. The driving law (16) can be interpreted as the AVs driving similarly to humans, but with an added tendency to maintain a uniform speed U, of which they may have knowledge via communication from other AVs or infrastructure. The AV controls are turned on at $t = 97\,\mathrm{minutes}$ (prior to that time, they are behaving like human-controlled vehicles), after the waves have fully developed, but they are only active when they are in the congested region.

Fig. 5a shows the initial phase of this simulation before the AVs have been activated. Obviously, it is the same result as in the non-AV simulation, shown in Fig. 4a. After the waves have developed and the AVs have been activated, Fig. 5b shows that the waves are less strong compared to the case with no AVs in Fig. 4b and the red curve is less oscillatory around the LWR solution. Finally, after a long enough time, in the presence of AVs, Fig. 5c shows that vehicle automation is successful at flow smoothing, as oscillations of the red curve are dampened and both the red and blue curves are closer to the LWR equilibrium solution.

The benefit of the AV-based flow smoothing is two-fold. First, the macroscopic traffic state in congestion is reverted back to being (almost) the equilibrium flow state, thus removing

the undesirable jam spillback that traffic waves produce. Second, traffic waves result in a significant increase in the energy demand of traffic flow, because vehicles constantly brake and accelerate. As a proof of concept to understand the impact on societal energy demand, we simply assume that all vehicles are identical combustion engine vehicles and use the vehicle energy model presented in [37] to compute the total fuel consumed by all vehicles on the road in the two scenarios simulated herein. The result is that in the absence of AVs, i.e., in traditional human-controlled traffic with fully established waves (shown in Figs. 4a–4c), the total fuel demand is 7164kg. In contrast, with active AV-based traffic control (shown in Figs. 5a–5c), the total fuel consumption reduces to 5250kg. This means that in the considered scenarios, traffic waves increase the overall energy demand of traffic by 36% (without any benefits), and AV-based control can save this wasted fuel.

6. Discussion

This study has highlighted that in vehicular traffic flow, the mesoscale of traffic waves can be of critical importance, both to the experience at the microscopic vehicle scale (persistent braking and accelerating) and to the macroscopic urban traffic scale (more splillback due to longer traffic jams). The analysis and simulations presented herein highlight that traffic waves can be traced back to dynamic instabilities that can occur both in microscopic models that explicitly resolve the individual vehicle dynamics, as well as in fluid dynamical models that circumvent the resolution of the vehicle scale. Moreover, the manifestation of traveling waves in the fundamental diagram of traffic flow has been highlighted, and its consequences on the effective densities and flow rates arising on the roadway.

A particular aspect showcased via the simulations is how field quantities at the meso- and the macro-scale can be systematically reconstructed from microscopic vehicle trajectories. These reconstructions have been applied to trajectories resulting from micro-simulations; however, they are in principle equally applicable to trajectories resulting from real traffic data. For trajectories that are governed by instabilities and traveling waves, reconstructions that capture the waves have been shown to produce characteristic straight lines in the fundamental diagram of traffic flow that intersect the equilibrium curve. Moreover, larger-scale reconstructions that average over the waves reveal that the resulting effective average state lies below the equilibrium curve. This means that non-equilibrium traffic flow is less efficient than equilibrium traffic flow, either by having a reduced flow rate at equal density, or by taking up more road space at equal throughput. This last situation is what has been demonstrated in the simulations shown herein: instabilities and waves cause longer traffic jams, and that can in the real world have significant adverse consequences on the flow across ramps upstream on the highway.

Finally, the simulations have demonstrated that the concept of Lagrangian flow smoothing, via a few well-controlled automated vehicles (here at 5% penetration rate), is valid: the presence of the AVs significantly dampens the traffic waves and produces a traffic state almost identical to what would arise under equilibrium conditions. Moreover, the simulations reveal that traffic waves result in a significant increase in the energy demand of traffic, and the associated consequences like emissions of greenhouse gases and other pollutants. Hence, traffic control strategies that can stabilize traffic flow and dampen waves can have a significant societal impact, both in terms of wealth and health. The mathematical models, and their analysis and simulation, showcased here are key building blocks towards developing and improving such strategies.

7. Acknowledgments

The authors would like to thank Rabie Ramadan for helpful discussions during the preparation of simulations of unstable traffic flow models. This material is based upon work supported by the U.S. Department of Energy's Office of Energy Efficiency and Renewable Energy (EERE) under the Vehicle Technologies Office award number CID DE-EE0008872. The views expressed herein do not necessarily represent the views of the U.S. Department of Energy or the United States Government.

References

[1] T. Alperovich and A. Sopasakis. Modeling highway traffic with stochastic dynamics. *J. Stat. Phys*, 133:1083–1105, 2008.
[2] A. Aw, A. Klar, T. Materne, and M. Rascle. Derivation of continuum traffic flow models from microscopic follow-the-leader models. *SIAM J. Appl. Math.*, 63(1):259–278, 2002.
[3] A. Aw and M. Rascle. Resurrection of second order models of traffic flow. *SIAM J. Appl. Math.*, 60:916–944, 2000.
[4] M. Bando, Hesebem K., A. Nakayama, A. Shibata, and Y. Sugiyama. Dynamical model of traffic congestion and numerical simulation. *Phys. Rev. E*, 51(2):1035–1042, 1995.
[5] N. Bellomo and C. Dogbe. On the modeling of traffic and crowds: A survey of models, speculations, and perspectives. *SIAM Rev.*, 53(3):409–463, 2011.
[6] G. Q. Chen, C. D. Levermore, and T. P. Liu. Hyperbolic conservation laws with stiff relaxation terms and entropy. *Comm. Pure Appl. Math.*, 47:787–830, 1994.
[7] R. M. Colombo. On a 2×2 hyperbolic traffic flow model. *Math. Comput. Modelling*, 35:683–688, 2002.
[8] C. F. Daganzo. The cell transmission model: A dynamic representation of highway traffic consistent with the hydrodynamic theory. *Transp. Res. B*, 28:269–287, 1994.
[9] C. F. Daganzo. In traffic flow, cellular automata = kinematic waves. *Transp. Res. B*, 40:396–403, 2006.
[10] L. C. Evans. *Partial differential equations*, volume 19 of *Graduate Studies in Mathematics*. American Mathematical Society, 1998.
[11] S. Fan, M. Herty, and B. Seibold. Comparative model accuracy of a data-fitted generalized Aw-Rascle-Zhang model. *Netw. Heterog. Media*, 9(2):239–268, 2014.
[12] S. Fan and B. Seibold. Data-fitted first-order traffic models and their second-order generalizations: Comparison by trajectory and sensor data. *Transportat. Res. Rec.*, 2391:32–43, 2013.
[13] S. Fan, Y. Sun, B. Piccoli, B. Seibold, and D. B. Work. A collapsed generalized Aw-Rascle-Zhang model and its model accuracy. *preprint*, 2017. `https://arxiv.org/abs/1702.03624`.
[14] M. R. Flynn, A. R. Kasimov, J.-C. Nave, R. R. Rosales, and B. Seibold. Self-sustained nonlinear waves in traffic flow. *Phys. Rev. E*, 79(5):056113, 2009.
[15] M. Fukui and Y. Ishibashi. Traffic flow in 1D cellular automaton model including cars moving with high speed. *J. Phys. Soc. Japan*, 65(6):1868–1870, 1996.
[16] S. K. Godunov. A difference scheme for the numerical computation of a discontinuous solution of the hydrodynamic equations. *Math. Sbornik*, 47:271–306, 1959.
[17] H. Greenberg. An analysis of traffic flow. *Oper. Res.*, 7:79–85, 1959.
[18] J. M. Greenberg. Extension and amplification of the Aw-Rascle model. *SIAM J. Appl. Math.*, 63:729–744, 2001.
[19] B. D. Greenshields. A study of traffic capacity. *Proceedings of the Highway Research Record*, 14:448–477, 1935.
[20] D. Helbing. Improved fluid-dynamic model for vehicular traffic. *Phys. Rev. E*, 51(4):3164–3169, 1995.
[21] D. Helbing. Traffic and related self-driven many-particle systems. *Reviews of Modern Physics*, 73:1067–1141, 2001.
[22] D. Helbing, A. Hennecke, V. Shvetsov, and M. Treiber. Micro- and macrosimulation of freeway traffic. *Mathematical and Computer Modelling*, 35(5):517–547, 2002.
[23] D. Helbing and A. F. Johansson. On the controversy around Daganzo's requiem for and Aw-Rascle's resurrection of second-order traffic flow models. *European Physical Journal B*, 69(4):549–562, 2009.
[24] R. Herman and I. Prigogine. *Kinetic theory of vehicular traffic*. Elsevier, New York, 1971.

[25] J.-C. Herrera, D. Work, X. Ban, R. Herring, Q. Jacobson, and A. Bayen. Evaluation of traffic data obtained via GPS-enabled mobile phones: The Mobile Century field experiment. *Transp. Res. B*, 18:568–583, 2010.
[26] S. P. Hoogendoorn and P. H. L. Bovy. Continuum modeling of multiclass traffic flow. *Transp. Res. B*, 34(2):123–146, 2000.
[27] R. Illner, A. Klar, and T. Materne. Vlasov-Fokker-Planck models for multilane traffic flow. *Commun. Math. Sci.*, 1(1):1–12, 2003.
[28] S. Jin and M. A. Katsoulakis. Hyperbolic systems with supercharacteristic relaxations and roll waves. *SIAM J. Appl. Math.*, 61:273–292, 2000.
[29] B. S. Kerner. Experimental features of the emergence of moving jams in free traffic flow. *J. Phys. A*, 33:221–228, 2000.
[30] B. S. Kerner and P. Konhäuser. Cluster effect in initially homogeneous traffic flow. *Phys. Rev. E*, 48:R2335–R2338, 1993.
[31] B. S. Kerner and P. Konhäuser. Structure and parameters of clusters in traffic flow. *Phys. Rev. E*, 50:54–83, 1994.
[32] A. Kesting, M. Treiber, and D. Helbing. General lane-changing model MOBIL for car-following models. *Transp. Res. Rec.*, 1999:86–94, 2007.
[33] T. S. Komatsu and S. Sasa. Kink soliton characterizing traffic congestion. *Phys. Rev. E*, 52:5574–5582, 1995.
[34] R. Krajewski, J. Bock, L. Kloeker, and L. Eckstein. The highD dataset: A drone dataset of naturalistic vehicle trajectories on german highways for validation of highly automated driving systems. In *2018 21st International Conference on Intelligent Transportation Systems (ITSC)*, pages 2118–2125, 2018.
[35] D. A. Kurtze and D. C. Hong. Traffic jams, granular flow, and soliton selection. *Phys. Rev. E*, 52:218–221, 1995.
[36] J.-P. Lebacque, S. Mammar, and H. Haj-Salem. Generic second order traffic flow modelling. In R. E. Allsop, M. G. H. Bell, and B. G. Heydecker, editors, *Transportation and Traffic Theory*, Proc. of the 17th ISTTT, pages 755–776. Elsevier, 2007.
[37] J. Lee and et al. Integrated framework of vehicle dynamics, instabilities, energy models, and sparse flow smoothing controllers. *DI-CPS'21: Proceedings of the Workshop on Data-Driven and Intelligent Cyber-Physical Systems*, pages 41–47, 2021.
[38] T. Li. Global solutions and zero relaxation limit for a traffic flow model. *SIAM J. Appl. Math.*, 61:1042–1061, 2000.
[39] T. Li and H. Liu. Stability of a traffic flow model with nonconvex relaxation. *Comm. Math. Sci.*, 3:101–118, 2005.
[40] M. J. Lighthill and G. B. Whitham. On kinematic waves. II. A theory of traffic flow on long crowded roads. *Proc. Roy. Soc. A*, 229(1178):317–345, 1955.
[41] T. P. Liu. Hyperbolic conservation laws with relaxation. *Comm. Math. Phys.*, 108:153–175, 1987.
[42] G. F. Newell. Nonlinear effects in the dynamics of car following. *Operations Research*, 9:209–229, 1961.
[43] G. F. Newell. A simplified theory of kinematic waves in highway traffic II: Queueing at freeway bottlenecks. *Transp. Res. B*, 27:289–303, 1993.
[44] P. Noble. Roll-waves in general hyperbolic systems with source terms. *SIAM J. Appl. Math.*, 67:1202–1212, 2007.
[45] M. Papageorgiou. Some remarks on macroscopic traffic flow modelling. *Transp. Res. A*, 32:323–329, 1998.
[46] Participants of the culminating workshop of the IPAM long program Fall 2015. White paper: New directions in mathematical approaches for traffic flow management. White paper, Institute for Pure and Applied Mathematics, 2015.
[47] H. J. Payne. Models of freeway traffic and control. *Proc. Simulation Council*, 1:51–61, 1971.
[48] H. J. Payne. FREEFLO: A macroscopic simulation model of freeway traffic. *Transp. Res. Rec.*, 722:68–77, 1979.
[49] W. F. Phillips. A kinetic model for traffic flow with continuum implications. *Transportation Planning and Technology*, 5:131–138, 1979.
[50] L. A. Pipes. An operational analysis of traffic dynamics. *Journal of Applied Physics*, 24:274–281, 1953.
[51] R. A. Ramadan, R. R. Rosales, and B. Seibold. Structural properties of the stability of jamitons. In Puppo G. and Tosin A., editors, *Mathematical Descriptions of Traffic Flow: Micro, Macro and Kinetic Models*, volume 12 of *SEMA SIMAI Springer Series*, pages 35–62. Springer, Cham, 2021.
[52] P. I. Richards. Shock waves on the highway. *Operations Research*, 4:42–51, 1956.

[53] S. Sakai, K. Nishinari, and S. IIda. A new stochastic cellular automaton model on traffic flow and its jamming phase transition. *J. Phys. A: Math. Gen.*, 39:15327–15339, 2006.
[54] B. Seibold, M. R. Flynn, A. R. Kasimov, and R. R. Rosales. Constructing set-valued fundamental diagrams from jamiton solutions in second order traffic models. *Netw. Heterog. Media*, 8(3):745–772, 2013.
[55] R. E. Stern, S. Cui, M. L. Delle Monache, R. Bhadani, M. Bunting, M. Churchill, N. Hamilton, R. Haulcy, H. Pohlmann, F. Wu, B. Piccoli, B. Seibold, J. Sprinkle, and D. B. Work. Dissipation of stop-and-go waves via control of autonomous vehicles: Field experiments. *Transp. Res. C*, 89:205–221, 2018.
[56] Y. Sugiyama, M. Fukui, M. Kikuchi, K. Hasebe, A. Nakayama, K. Nishinari, S. Tadaki, and S. Yukawa. Traffic jams without bottlenecks – Experimental evidence for the physical mechanism of the formation of a jam. *New Journal of Physics*, 10:033001, 2008.
[57] M. Treiber, A. Hennecke, and D. Helbing. Congested traffic states in empirical observations and microscopic simulations. *Physical Review E*, 62(2):1805–1823, 2000.
[58] R. Underwood. Speed, volume, and density relationships: Quality and theory of traffic flow. Technical report, Yale Bureau of Highway Traffic, 1961.
[59] Federal Highway Administration US Department of Transportation. Next Generation Simulation (NGSIM). Website. `http://ops.fhwa.dot.gov/trafficanalysistools/ngsim.htm`.
[60] Y. Wang and M. Papageorgiou. Real-time freeway traffic state estimation based on extended Kalman filter: A general approach. *Transp. Res. B*, 39:141–167, 2005.
[61] G. B. Whitham. Some comments on wave propagation and shock wave structure with application to magnetohydrodynamics. *Comm. Pure Appl. Math.*, 12:113–158, 1959.
[62] G. B. Whitham. *Linear and nonlinear waves*. John Wiley and Sons, New York, 1974.
[63] R. E. Wilson and J. A. Ward. Car-following models: fifty years of linear stability analysis – A mathematical perspective. *Transportation Planning and Technology*, 34(1):3–18, 2011.
[64] D. Work, O.-P. Tossavainen, S. Blandin, A. Bayen, T. Iwuchukwu, and K. Tracton. An ensemble Kalman filtering approach to highway traffic estimation using GPS enabled mobile devices. In *47th IEEE Conference on Decision and Control*, pages 5062–5068, Cancun, Mexico, 2008.
[65] F. Wu, R. E. Stern, S. Cui, M. L. Delle Monache, R. Bhadani, M. Bunting, M. Churchill, N. Hamilton, R. Haulcy, B. Piccoli, B. Seibold, J. Sprinkle, and D. B. Work. Tracking vehicle trajectories and fuel rates in phantom traffic jams: Methodology and data. *Transp. Res. C*, 99:82–109, 2019.
[66] H. M. Zhang. A non-equilibrium traffic model devoid of gas-like behavior. *Transp. Res. B*, 36:275–290, 2002.

(Nour Khoudari) Department of Mathematics, Temple University,
1805 North Broad Street, Philadelphia, PA 19122

Email address: `nour.khoudari@temple.edu`

(Benjamin Seibold) Department of Mathematics, Temple University,
1805 North Broad Street, Philadelphia, PA 19122

Email address: `seibold@temple.edu`

URL: `http://www.math.temple.edu/~seibold`